SCIENTIFIC REPORTS

OPEN

SUBJECT AREAS:
MICROFLUIDICS
ELECTRONIC PROPERTIES AND MATERIALS
CHEMICAL ENGINEERING
SOLAR CELLS

Received
11 June 2013

Accepted
17 July 2013

Published
5 August 2013

Correspondence and requests for materials should be addressed to O.D.V. (odvelev@ncsu.edu)

* Current address: Department of Materials Science and Engineering, University of Illinois at Urbana-Champaign, Urbana, IL 61801-2325, USA.

Regenerable Photovoltaic Devices with a Hydrogel-Embedded Microvascular Network

Hyung-Jun Koo* & Orlin D. Velev

Department of Chemical & Biomolecular Engineering, North Carolina State University, Raleigh, NC 27695-7905, USA.

Light-driven degradation of photoactive molecules could be one of the major obstacles to stable long term operation of organic dye-based solar light harvesting devices. One solution to this problem may be mimicking the regeneration functionality of a plant leaf. We report an organic dye photovoltaic system that has been endowed with such microfluidic regeneration functionality. A hydrogel medium with embedded channels allows rapid and uniform supply of photoactive reagents by a convection-diffusion mechanism. A washing-activation cycle enables reliable replacement of the organic component in a dye-sensitized photovoltaic system. Repetitive restoration of photovoltaic performance after intensive device degradation is demonstrated.

Photovoltaic systems based on photosensitive organic dye molecules could be a simple and economical alternative to conventional solar cells, and have been actively developed for decades[1–3]. The best examples of such devices are the common dye-sensitized solar cells (DSSCs)[4,5], though other systems based on a dye-embedded hydrogel or naturally derived photoactive molecules have also been reported recently[6–8]. Since the organic dyes are generally susceptible to light, high temperature or water, however, the degradation of photoactive molecules in the dye-based photovoltaic systems could be a critical problem, which leads to deterioration of the long-term performance of these photovoltaic cells[9–16].

Photosystems, which are organic photoactive complexes forming the core of plant leaves involved in photosynthesis, also suffer from light-induced damage. When the photosystems are irreversibly damaged by light stress, a leaf disassembles the damaged components in the photosystems and replaces them with newly biosynthesized ones[17]. The replication of this self-regeneration process existing in natural leaves into human-made devices could be the key to making the next generation of robust and reliable photovoltaics. One key example by Ham et al. is a report of the synthesis of a photoelectrochemical complex broadly mimicking the regeneration process of a leaf[18]. The molecular assembly/disassembly of the components, such as lipids, proteins, carbon nanotubes and photosynthetic reaction centre, is reversibly controlled by presence or absence of surfactants.

The uniform distribution and circulation of water, ions and photosynthate in natural leaves are enabled by their venation network. This natural "microfluidic" channel structure facilitates the basic functions of a leaf including photosynthesis and enables the regeneration of photoactive molecules[19,20]. We present a practical prototype of biomimetic photovoltaic devices with structure mimicking this regeneration functionality of a plant leaf. The device is based on a naturally derived agarose hydrogel, with embedded network of microfluidic channels. The principles of transport of the photoactive reagents, dye and electrolytes, supplied into the microfluidic network will be discussed. We report a simple and reliable process for the regeneration of this microfluidic hydrogel solar cell by controlling the pH-dependent desorption/adsorption kinetics of the dye molecules on the photoanode. Finally, we demonstrate the photocurrent recovery of the biomimetic solar cells damaged by intense UV illumination.

Results

Design of biomimetic microvascular network and dye infusion. The device is generating photocurrent similarly to a common DSSC system, however it includes a matrix of hydrogel with microchannels allowing dye infusion and replenishment. The structure of the photovoltaic device with the microfluidic network embedded in hydrogel (μ-fluidic gel photovoltaics, μ-FGPVs) is shown in Figure 1. Nanoporous TiO_2 thin film and platinum catalysts were deposited on two fluorine-doped tin oxide (FTO) glass substrates, which

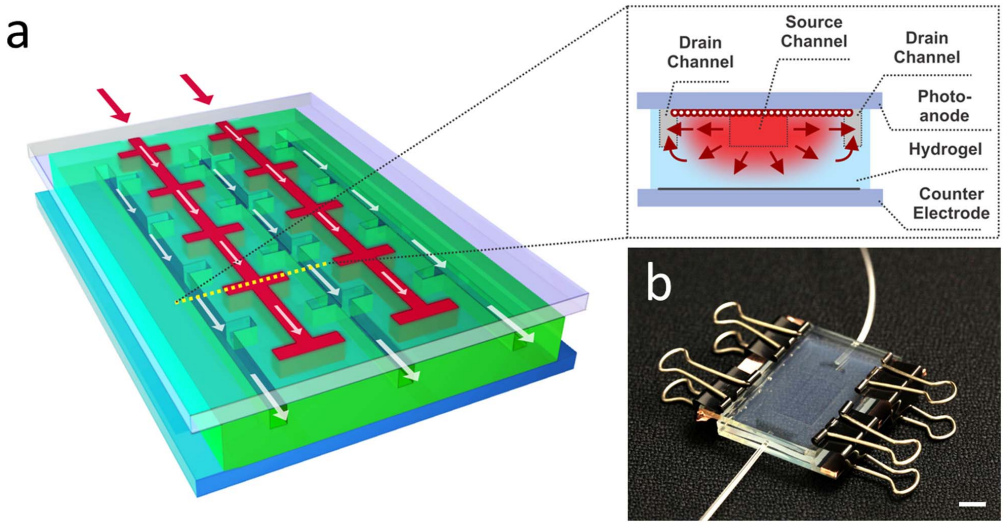

Figure 1 | A biomimetic photovoltaic device with microfluidic replenishment network. (a) A schematic of microfluidic channel network within the hydrogel photovoltaics (μ-FGPVs). The white arrows indicate the convection-dominant transport of dye and electrolyte molecules along the microfluidic channels. The inset displays the cross section view across the dotted yellow line. TiO_2 nanoparticles and Pt catalysts are deposited on the photoanode and the counter electrode, respectively. The red arrows indicate the lateral diffusive/convective transport between the source channels and drain channels. (b) A photograph of the prototype μ-FGPVs device. The top electrode is the photoanode. Scale bar = 1 cm. The area and the thickness of TiO_2 film are 3 cm^2 and ~6 μm, correspondingly.

were used as a photoanode and a counter electrode, respectively. The 2 wt.% agarose gel layer with interdigitated microfluidic channels was fabricated by replica molding. The hot liquefied agarose aqueous solution (in deionized water) was poured on a patterned SU-8 mold and was cooled down to room temperature and gelled. The hydrogel layer with the embedded channel network is sandwiched between the photoanode and the counter electrode. The reagents needed for the photovoltaic operation, photosensitive dyes and electrolytes, could be infused, removed and replenished uniformly via the network of interdigitated main channels with secondary branches as shown in Figure 1. The channels are facing the TiO_2 film to facilitate the adsorption and desorption of the dyes.

The μ-FGPV prototypes shown in Figure 1 use the organic dye Eosin Y as an inexpensive and reasonably efficient photosensitive reagent[21–23]. The dye was injected into the prototype devices in the form of an aqueous solution containing 0.005 M Eosin Y, 0.6 M potassium iodide and 0.03 M iodine. Snapshots of the first infusion of the device by dye and electrolyte solution at an injection rate of 10 μl/min are shown in Figure 2(a). The solution first flows along the source channels, followed by penetration through the gel to reach the drain channels. The dye and the electrolytes are delivered predominantly by convective transport along the channels, whereas both convection and diffusion become comparably important in the penetration of those reagents through the gel. A finite-element simulation using COMSOL Multiphysics package (COMSOL Inc., Burlington, MA) proves the beneficial effect of channel interdigitation and branching on the reagent distribution (see the simulation description and Supplementary Fig. S1 in Supplementary Information). We compared the uniformity of the coverage of the supplied reagents in different channel designs 1 hr after the reagents are supplied. The simulation results prove that the interdigitated channels with secondary side branches provide the most uniform

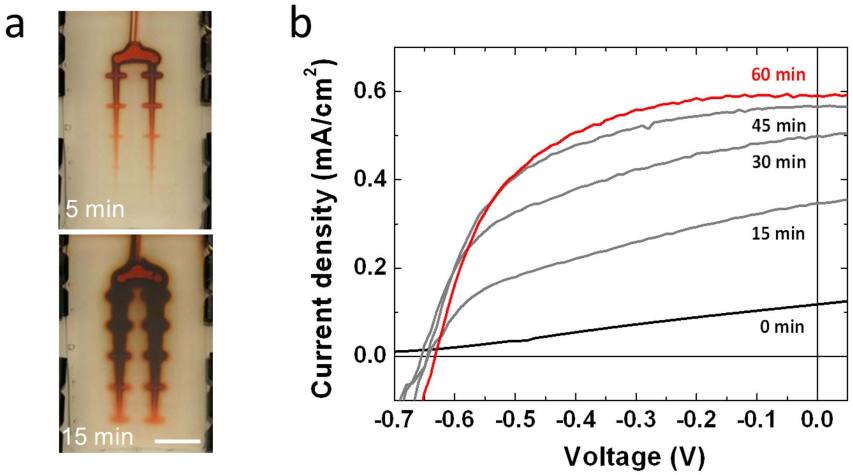

Figure 2 | Initial infusion of organic dye into μ-FGPVs and resulting increase in photovoltaic performance. (a) Images illustrating the progressive infusion of dye and electrolytes through the gel-vascular network at 5 and 15 min after injection of the solution. Scale bar = 1 cm (see Supplementary Fig. S3 for more snapshots of the solute distribution at different times). The injection rate is 10 μl/min. (b) I–V curves of the μ-FGPVs under illumination after the first injection of the aqueous solution of dye and electrolytes.

reagent coverage among the channel designs. The simulation yielded a Peclet number (Pe) – a dimensionless number representing the ratio of the convection rate to the diffusion rate, $Pe = \frac{Lv}{D}$, where L, v and D is the hydraulic diameter, the velocity and the diffusion coefficient, respectively – in the gel of Pe ~ 3, which is much lower than the value of 110 ~ 140 in the channels (See Supplementary Fig. S2). Since the diffusion is driven by the concentration gradient, the enhanced diffusive transport in the porous gel media could facilitate uniform distribution of the reagent while the convection-dominant transport in the channels allows for the rapid supply. Such convective/diffusive transport mechanism is typical for hydrated porous gel media[24] and, notably, important principle of leaf supply in a plant[25,26].

Photovoltaic performance of the microfluidic solar cells. To investigate how the dye and electrolytes infused through the microfluidic network contribute to the photovoltaic operation, we measured the current density of the μ-FGPVs as a function of the applied voltage under illumination during the supply of the reagents (Figure 2(b)). The current and voltage generation at 0 min ($J_{sc} \cong 0.1$ mA/cm^2, $V_{oc} \approx 0.7$ V) possibly results from photoelectrochemical oxidation of water under the illuminated condition. The short-circuit current density (J_{sc}) increases as a solution of dye and electrolytes is freshly infused, while the open-circuit voltage (V_{oc}) barely changes during the infusion progress. This is because J_{sc} mostly depends on the amount of the dye molecules adsorbed on the TiO_2 surface[27], whereas V_{oc} is determined by the energy difference between the Fermi-level of the TiO_2 electrode and the redox potential of the electrolytes[28]. The J_{sc} is saturated at 60 min after the injection, at which time the dye and electrolytes appear to have reached adsorption equilibria at the TiO_2 photoanode. The steady-state J_{sc}, V_{oc}, fill factor and efficiency are 0.59 mA/cm^2, 630 mV, 0.57 and 0.21%, respectively. These performance values are lower than ones with expensive rare-metal-based dyes such as N719 and nonaqueous volatile solvents, but are reasonable for a device with water-based electrolyte and common organic dye[21,29]. Also, the area of TiO_2 film of the μ-FGPV prototype (3 cm^2) is one order of magnitude larger than that of most devices reported for academic research[30–32]. It is known that the apparent photocurrent, and therefore the resulting efficiency, decreases as the active area of TiO_2 increases[33]. After assuring that these devices have reasonable performance characteristics, we challenge them by accelerated photodegradation and use the microfluidic network as means of their regeneration.

Photocurrent regeneration in the microfluidic photovoltaics. When the dye solution is first introduced to the pristine TiO_2 film in Figure 2, the Eosin Y molecules are chemically bound to the TiO_2 surface. The chemisorbed dye molecules are excited by absorbing photons and inject electrons into the conduction band of the TiO_2 to generate electricity[34]. The microfluidic network allowed for a robust regeneration process schematically described in Figure 3(a), by removing and replenishing on demand the organic dye in the

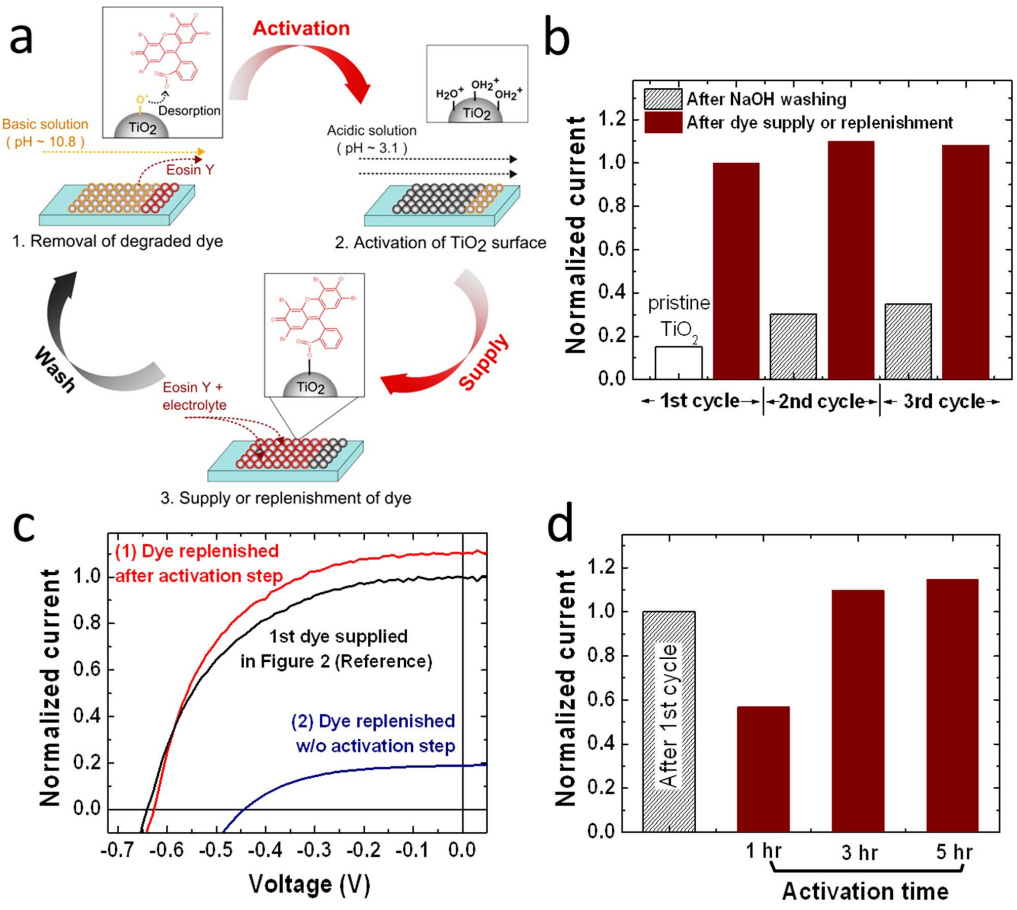

Figure 3 | Replacement procedure of the organic photovoltaic dye during μ-FGPVs regeneration. (a) Schematics of the three-step regeneration process. (b) Photocurrent generated by the μ-FGPVs during three subsequent cycles of washing and replenishment of the dye/electrolyte solution. (c) I–V curves of the dye-replenished μ-FGPVs with and without the activation step, showing that the activation process is essential. The device for the curve (1) was washed with aqueous NaOH solution for 3 hrs, followed by treating with HCl solution for 3 hrs before the dye replenishment. The device characterized by curve (2) was washed with aqueous NaOH solution for 6 hrs before dye replenishment. All samples were characterized after the 1 hr dye-supply step. (d) Effect of the activation duration on the regeneration efficiency of the μ-FGPVs. The injection rate of all solutions in (b)–(d) is 10 μl/min.

photoactive layer. The adsorption/desorption rate of the photoactive dye molecules on the TiO_2 surfaces depends on the pH of the environment, which thus becomes the key parameter for control of the replenishment process. The regeneration begins with the step 1 of injection of basic aqueous NaOH solution with pH 10.8. Since the isoelectric point of TiO_2 is 6.2 and the pKa of Eosin Y is 4.8, the similarly ionized dye molecules are desorbed from the TiO_2 film under basic pH environment[34]. The desorbed dye molecules and the electrolytes are washed out by the flowing basic solution. The TiO_2 treated with the basic solution acquires a negatively charged surface. This charge would hinder the re-adsorption of the fresh Eosin Y molecules, which are also negatively charged, because of electrostatic repulsion. To reverse the surface charge of the TiO_2, an acidic aqueous HCl solution with pH 3.1 is injected in the step 2 of an "activation" process. The TiO_2 activation might be speeded by acidic treatment at lower pH. However, the Eosin Y molecules in solution injected after activation with acidic solutions below pH ≈ 3 were prone to aggregation because of reduced charge-charge repulsion between the dye molecules. The activated TiO_2 film has a positively charged surface, where the slightly negatively charged Eosin Y molecules readily adsorb when a solution of the fresh dye and electrolytes is infused during step 3. The photocurrents generated by μ-FGPVs during three consequent washing/replenishment cycles are shown in Figure 3(b), demonstrating that the J_{sc} is reliably recovered during the regeneration process.

The importance of the activation step is illustrated in Figure 3(c), where we compare the recovery of the photocurrent generation of the μ-FGPVs with and without the acid treatment step. When the solution of dye and electrolytes is re-supplied after the regeneration process, the photocurrent in μ-FGPVs is more than 100% recovered only after *both* washing and activation processes, while little recovery of the photocurrent is observed in a device without acid activation. The ~10% increase of the photocurrent after the regeneration process is possibly a result of enhanced dye adsorption because of the surface charge modification (note that the as-deposited TiO_2 film was not treated with acid solution before the first dye supply). We also investigated the effect of the duration of the activation step on the photocurrent recovery (Figure 3(d)). The injection time of the acidic solution was varied from 1 to 5 hrs at a rate of 10 μl/min. The photocurrent was completely recovered when the TiO_2 is exposed to the solution for more than 3 hrs. Less than 60% recovery of the photocurrent was recorded with the activation process lasting for 1 hr. Thus, an activation step of certain duration is essential for completion of the regeneration process. The minimum required activation time may potentially be shortened by higher injection rate of the acidic solution.

We practically demonstrated the regeneration functionality of the μ-FGPVs by replacing light-damaged photosensitive molecules with a stock of fresh ones. To accelerate the degradation process, the device was illuminated with intense UV light source (100 W Hg vapor short arc lamp, λ: 320 ~ 500 nm). The effect of UV illumination time on the photovoltaic performance of the μ-FGPVs is shown in Supplementary Fig. S4. The photocurrent plummeted during the UV illumination, due to the photo-degradation of the Eosin Y dye molecules. The photocurrent measured during two UV-degradation/regeneration cycles is plotted in Figure 4. It decreased by ~40% after the device was illuminated with UV for 10 min, but was recovered during the successive regeneration process of washing, activation and dye-replenishment. During the second cycle, the photocurrent decreased by about 60% during the UV illumination for 30 min, but is also completely restored. No significant deterioration of the TiO_2 film and the hydrogel was observed during the regeneration cycles. Thus, the microfluidic regeneration allows the photodegraded organic molecules in the μ-FGPVs to be repeatedly replaced and the device performance to be recovered.

Discussion

A plant in nature maintains its photosynthetic activity by continually rehydrating and regenerating the photoactive complexes in leaves through a venation network. We report here a regenerable photovoltaic device that broadly mimics this functionality by using hydrogel with embedded microfluidic channels. The convective-diffusive transport of solutes in the microfluidic hydrogel enables the uniform supply of the photoactive dye molecules and electrolyte into the

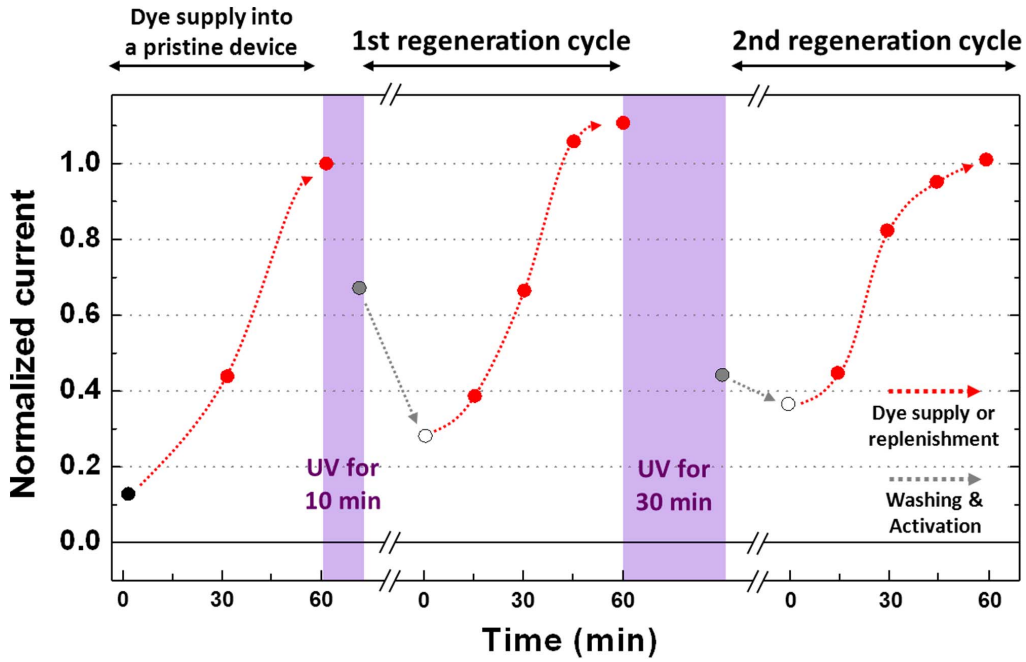

Figure 4 | Demonstration of the regeneration functionality of μ-FGPVs. The data confirm the regeneration and photocurrent recovery of the μ-FGPVs after accelerated degradation of the dye molecules by illumination with intense UV light. The violet-colored regions represent the periods of intense illumination. The dotted arrows are guides to the eye. The washing and activation steps were performed for 5 hrs each.

device. After the reagents are delivered, the key effect that enables a reliable process for dye replacement is the pH-dependent desorption/re-adsorption of the dye molecules on the TiO_2 photoanodes. We demonstrate device regeneration and recovery of the photocurrent after the μ-FGPVs were subjected to accelerated degradation with intense UV light. The materials and the fabrication process of the regenerative μ-FGPVs are inexpensive and scalable. The use of soft lithography for making the channels makes possible the design of potentially more efficient (e.g. fractal-like) channel networks. The device is made of rare-metal-free organic dyes and naturally derived water gel, which could reduce its environmental footprint. One of the most distinctive features of the μ-FGPVs is their "open-fluidic" design, as opposed to the closed structure of conventional photovoltaic devices. The ease of supply and drainage of a liquid solution in the fluidic system may ameliorate the electrolyte leakage problem, which is one of the serious hurdles to making the conventional DSSCs practical[35,36].

A couple of challenges have to be addressed in the further development of such photovoltaic systems. The low photoconversion efficiency can be increased by traditional approaches such as molecular engineering of dye, manipulation of the TiO_2 nanostructure and optimization of electrolyte composition as well as new solutions, for example, the use of conducting or semiconducting hydrogel as an additional high-surface photoanode[37]. Another challenge is that these μ-FGPVs require an external pump for reagent supply, which complicates their design and operation. One potential solution can also be found in nature, where the pressure drop in the xylem of a plant driven by water evaporation pulls up the water from the soil[38]. Replicating of such transpiration mechanisms could allow future regenerative devices to operate autonomously. Overall, we believe that such designs point a way for development of improved biomimetic leaf-like photovoltaics.

Methods

Materials. Eosin Y, Chloroplatinic acid (H_2PtCl_6), potassium iodide (KI) and iodine (I_2) were purchased from Sigma-Aldrich. All chemicals were used without any further purification. SU-8 100 photoresist was obtained from Microchem. Agarose (biochemistry research grade) was purchased from Acros Organics. Fluorine doped tin oxide glass (FTO glass, TEC-8, 2.3 mm thick) was purchased from Hartford Glass Inc. A screen-printable TiO_2 paste (Ti-Nanoxide T20) was obtained from Solaronix. Deionized water ($R \geq 18$ MΩ cm) was produced with a Millipore Synergy Water purification system.

Device fabrication of μ-FGPVs. The nanoporous TiO_2 film is prepared on the FTO photoanode by doctor-blading of the TiO_2 paste, followed by sintering at 500 °C for 90 min. The TiO_2 film has an area of 3 cm^2 and a thickness ~6 μm. The platinum catalysts are deposited on the counter electrode by spin-coating of 0.7 mM H_2PtCl_6 solution, followed by heating at 400 °C for 20 min. The agarose gel layer with interdigitated microfluidic channels is prepared by replica molding. The hot liquefied agarose aqueous solution (2 wt.% in deionized water) was poured on a patterned SU-8 mold and was cooled down to room temperature. The mold with the micro pattern was fabricated by a photolithographic technique. SU-8 100 photoresist was coated on a silicon wafer to a thickness of ~250 μm using a spin-coater (Model P6700, Specialty Coating Systems, Inc.). The photomask with the interdigitated channel pattern was placed on the soft-baked photoresist, followed by UV exposure (IntelliRay UV Flood Curing System, Uvitron). The final mold with the channel pattern was obtained after the post exposure bake and development.

The μ-FGPVs was fabricated by sandwiching the hydrogel layer with embedded microfluidic channels between the photoanode and the counter electrode. The hydrogel layer was enclosed in a PDMS spacer and two Tygon tubes were inserted into the spacer as an inlet and an outlet. The aqueous solution of 5 mM Eosin Y dye and electrolyte (0.6 M KI and 0.03 M I_2) was injected into the microfluidic hydrogel at a rate of 10 μl/min by a syringe pump (NE-1800, New Era Pump System Inc.). Aqueous acidic and basic solutions were also injected at the same flow rate.

Numerical simulation. The fluid characteristics and the solute transport were simulated with COMSOL Multiphysics package ver. 3.5. The Brinkman equation, the Navier-Stokes equation and the convection/diffusion equation were used as predefined in COMSOL. The stationary solver was chosen for the Brinkman equation and the Navier-Stokes equation and the time-dependent solver was chosen for the convection/diffusion equation. The detailed information about the equations, the physical properties of domains and the boundary conditions used for the simulation study can be found in Supplementary Information.

Characterization. The photocurrent/photovoltage of the device were measured by using a computer-controlled source meter (Keithley 2400, Keithley Instruments Inc.) under illumination by a solar simulator (Model-91160 equipped with 300 W Xenon lamp, Newport). The light intensity was adjusted using a calibrated Si standard solar cell (91150V, Newport) to 100 mW/cm^2 and AM 1.5 G one sun light condition before every measurement. To accelerate the degradation process, the device was illuminated with intense UV light source (OmniCure S1000, High pressure 100 W Hg vapor short arc lamp, λ: 320 ~ 500 nm, Lumen Dynamics Inc.). The distance between the UV light source and the device was 10 cm.

1. Memming, R. Photochemical and electrochemical processes of excited dyes at semiconductor and metal electrodes. *Photochem. Photobiol.* **16**, 325–333 (1972).
2. Tsubomura, H., Matsumura, M., Nomura, Y. & Amamiya, T. Dye sensitised zinc oxide: aqueous electrolyte: platinum photocell. *Nature* **261**, 402–403 (1976).
3. Matsumura, M., Nomura, Y. & Tsubomura, H. Dye-sensitization on the photocurrent at zinc oxide electrode in aqueous electrolyte solution. *B. Chem. Soc. Jpn.* **50**, 2533–2537 (1977).
4. O'Regan, B. & Grätzel, M. A low-cost, high-efficiency solar cell based on dye-sensitized colloidal TiO_2 films. *Nature* **353**, 737–740 (1991).
5. Grätzel, M. Photoelectrochemical cells. *Nature* **414**, 338–344 (2001).
6. Koo, H.-J., Chang, S. T., Slocik, J. M., Naik, R. R. & Velev, O. D. Aqueous soft matter based photovoltaic devices. *J. Mater. Chem.* **21**, 72–79 (2011).
7. Yehezkeli, O. *et al.* Integrated photosystem II-based photo-bioelectrochemical cells. *Nat. Commun.* **3**, 742 (2012).
8. Mershin, A. *et al.* Self-assembled photosystem-I biophotovoltaics on nanostructured TiO_2 and ZnO. *Sci. Rep.* **2**, 234 (2012).
9. Hinsch, A. *et al.* Long-term stability of dye-sensitised solar cells. *Prog. Photovolt. Res. Appl.* **9**, 425–438 (2001).
10. Agrell, H. G., Lindgren, J. & Hagfeldt, A. Degradation mechanisms in a dye-sensitized solar cell studied by UV-VIS and IR spectroscopy. *Sol. Energy* **75**, 169–180 (2003).
11. Uam, H.-S., Jung, Y.-S., Jun, Y. & Kim, K.-J. Relation of Ru(II) dye desorption from TiO_2 film during illumination with photocurrent decrease of dye-sensitized solar cells. *J. Photoch. Photobio. A* **212**, 122–128 (2010).
12. Sommeling, P. M., Späth, M., Smit, H. J. P., Bakker, N. J. & Kroon, J. M. Long-term stability testing of dye-sensitized solar cells. *J. Photoch. Photobio. A* **164**, 137–144 (2004).
13. Grätzel, M. Conversion of sunlight to electric power by nanocrystalline dye-sensitized solar cells. *J. Photoch. Photobio. A* **164**, 3–14 (2004).
14. Grünwald, R. & Tributsch, H. Mechanisms of instability in Ru-based dye sensitization solar cells. *J. Phys. Chem. B* **101**, 2564–2575 (1997).
15. Nour-Mohhamadi, F., Nguyen, S. D., Boschloo, G., Hagfeldt, A. & Lund, T. Determination of the light-induced degradation rate of the solar cell sensitizer N719 on TiO_2 nanocrystalline particles. *J. Phys. Chem. B* **109**, 22413–22419 (2005).
16. Toivola, M., Peltokorpi, L., Halme, J. & Lund, P. Regenerative effects by temperature variations in dye-sensitized solar cells. *Sol. Energ. Mat. Sol. Cells* **91**, 1733–1742 (2007).
17. Aro, E.-M., Virgin, I. & Andersson, B. Photoinhibition of Photosystem II. Inactivation, protein damage and turnover. *BBA-Bioenergetics* **1143**, 113–134 (1993).
18. Ham, M.-H. *et al.* Photoelectrochemical complexes for solar energy conversion that chemically and autonomously regenerate. *Nat. Chem.* **2**, 929–936 (2010).
19. Evert, R. F. *Esau's Plant Anatomy: Meristems, Cells, and Tissues of the Plant Body: Their Structure, Function, and Development* 3rd edn 1–13 (John Wiley & Sons, Inc., 2006).
20. Blonder, B., Violle, C., Bentley, L. P. & Enquist, B. J. Venation networks and the origin of the leaf economics spectrum. *Ecol. Lett.* **14**, 91–100 (2011).
21. Wang, Z.-S., Sayama, K. & Sugihara, H. Efficient Eosin Y Dye-sensitized solar cell containing Br^-/Br_3^- Electrolyte. *J. Phys. Chem. B* **109**, 22449–22455 (2005).
22. Lee, W.-J., Okada, H., Wakahara, A. & Yoshida, A. Structural and photoelectrochemical characteristics of nanocrystalline ZnO electrode with Eosin-Y. *Ceram. Int.* **32**, 495–498 (2006).
23. Guillén, E. *et al.* Photovoltaic performance of nanostructured zinc oxide sensitised with xanthene dyes. *J. Photoch. Photobio. A* **200**, 364–370 (2008).
24. Choi, N. W. *et al.* Microfluidic scaffolds for tissue engineering. *Nat. Mater.* **6**, 908–915 (2007).
25. Noblin, X. *et al.* Optimal vein density in artificial and real leaves. *Proc. Natl. Acad. Sci.* **105**, 9140–9144 (2008).
26. Zhou, H. *et al.* Leaf-architectured 3D Hierarchical Artificial Photosynthetic System of Perovskite Titanates Towards CO_2 Photoreduction Into Hydrocarbon Fuels. *Sci. Rep.* **3**, 1667 (2013).
27. Koo, H.-J. *et al.* Nano-embossed hollow spherical TiO_2 as bifunctional material for high-efficiency dye-sensitized solar cells. *Adv. Mater.* **20**, 195–199 (2008).
28. Pichot, F. & Gregg, B. A. The photovoltage-determining mechanism in dye-sensitized solar cells. *J. Phys. Chem. B* **104**, 6–10 (1999).
29. Murakami, T. N., Saito, H., Uegusa, S., Kawashima, N. & Miyasaka, T. Water-based dye-sensitized solar cells: Interfacial activation of TiO_2 mesopores in contact with aqueous electrolyte for efficiency development. *Chem. Lett.* **32**, 1154–1155 (2003).

30. Kim, D. H. *et al.* Stable anatase TiO_2 coating on quartz fibers by atomic layer deposition for photoactive light-scattering in dye-sensitized solar cells. *Nanoscale* **4**, 4731–4738 (2012).
31. Yang, L. & Leung, W. W.-F. Electrospun TiO_2 nanorods with carbon nanotubes for efficient electron collection in dye-sensitized solar cells. *Adv. Mater.* **25**, 1792–1795 (2013).
32. Cho, T.-Y., Han, C.-W., Jun, Y. & Yoon, S.-G. Formation of artificial pores in nano-TiO_2 photo-electrode films using acetylene-black for high-efficiency, dye-sensitized solar cells. *Sci. Rep.* **3**, 1496 (2013).
33. Park, J. *et al.* On the I–V measurement of dye-sensitized solar cell: Effect of cell geometry on photovoltaic parameters. *Sol. Energ. Mat. Sol. Cells* **91**, 1749–1754 (2007).
34. Wang, Q., Chen, C., Zhao, D., Ma, W. & Zhao, J. Change of adsorption modes of dyes on fluorinated TiO_2 and its effect on photocatalytic degradation of dyes under visible irradiation. *Langmuir* **24**, 7338–7345 (2008).
35. Bai, Y. *et al.* High-performance dye-sensitized solar cells based on solvent-free electrolytes produced from eutectic melts. *Nat. Mater.* **7**, 626–630 (2008).
36. Chung, I., Lee, B., He, J., Chang, R. P. H. & Kanatzidis, M. G. All-solid-state dye-sensitized solar cells with high efficiency. *Nature* **485**, 486–489 (2012).
37. Pan, L. *et al.* Hierarchical nanostructured conducting polymer hydrogel with high electrochemical activity. *Proc. Natl. Acad. Sci.* **109**, 9287–9292 (2012).
38. Wheeler, T. D. & Stroock, A. D. The transpiration of water at negative pressures in a synthetic tree. *Nature* **455**, 208–212 (2008).

Acknowledgements

The support from the NSF Triangle MRSEC for Programmable Soft Matter (DMR-1121107), the NSF-ASSIST Nanosystems Engineering Research Center (EEC-1160483) and DOE (08NT0001925) is gratefully acknowledged.

Author contributions

H.-J.K. and O.D.V. designed the experiments. H.-J.K. conducted the experiments and the numerical simulations. H.-J.K. and O.D.V. analyzed the data and wrote the manuscript.

Additional information

Supplementary information accompanies this paper at http://www.nature.com/scientificreports

Competing financial interests: The authors declare no competing financial interests.

How to cite this article: Koo, H.-J. & Velev, O.D. Regenerable Photovoltaic Devices with a Hydrogel-Embedded Microvascular Network. *Sci. Rep.* **3**, 2357; DOI:10.1038/srep02357 (2013).